

**Discrete model analysis of the critical current density
measurements in superconducting thin films by a single coil
inductive method**

M. Aurino¹, E. Di Gennaro¹, F. Di Iorio¹, A. Gauzzi², G. Lamura^{1,*} and A. Andreone¹

¹*CNR-I.N.F.M. COHERENTIA and Dipartimento Scienze Fisiche,*

Università di Napoli Federico II, I-80125, Napoli, Italy.

²*Istituto Materiali per Elettronica e Magnetismo - Consiglio Nazionale delle Ricerche,*

Area delle Scienze, 43010 Parma, Italy.

(Dated: August 8, 2005)

Abstract

The critical current density of a superconducting film can be easily determined by an inductive and contactless method. Driving a sinusoidal current in a single coil placed in front of a superconducting sample, a non zero third harmonic voltage V_3 is induced in it when the sample goes beyond the Bean critical state. The onset of V_3 marks the value of current beyond which the sample response to the magnetic induction is no more linear. To take into account, in a realistic way, the magnetic coupling between the film and the coil we have developed a discrete model of the inducing and induced currents distribution. In the framework of this model the magnetic field profile on the sample surface and the coefficient linking the current flowing in the coil and the critical current density J_C of superconducting thin films is evaluated. The numerical results are checked measuring J_C of several thin films of $YBa_2Cu_3O_{7-\delta}$ of known superconducting properties, used as a control material.

PACS numbers: 74.25.-q,74.25.Fy,74.25.sv,74.25.Nf

I. INTRODUCTION

The use of superconductors in engineering applications like high field superconducting magnets is of fundamental importance. For this reason the critical current density is a relevant figure of merit, that needs to be measured in samples of different nature and shapes like sintered pellets, tapes or thin films. In particular, the development of flat cables for superconducting magnets requires a flexible and reliable measurement of this transport property without damaging the sample.

Years ago Claassen *et al.*¹ proposed a non destructive and contactless method to measure J_C in superconducting thin films. This method was theoretically justified², subsequently extended for the analysis of bulk superconductors³, and then used for the determination of the current-voltage characteristics of superconducting thin films⁴. The basic principle is the following: a small coil, placed in close contact with the sample under test, is excited injecting a sinusoidal current $I_0 \cos \omega t$, and an ac magnetic field is generated. The linear and nonlinear response of the superconducting film is then collected by the same coil. The critical current density J_C is determined by looking at the behaviour of the induced third harmonic signal $V_3 \cos(3\omega t)$ as a function of the inducing current. The link between J_C and the current circulating in the probe coil is found^{1,2} by assuming two important conditions: *i)* the sample surface is flat and extended to infinity in two dimensions; *ii)* the total induction field is zero on the back side of the sample. Of course this last condition follows from the first one when the magnetic penetration depth $\lambda \leq d$, where d is the sample thickness. Due to these assumptions, the field profile must have as boundary condition that only the parallel component is nonzero at the sample surface. By using a "mirror technique", the sample is replaced by an image coil reflected by the sample surface and carrying the same current. In this case the total induction field on the sample surface is just twice the value that would be generated by the single coil in the absence of the screening currents. According to *ii)* and the Ampère's law, the maximum sheet current K_S that can be sustained by a superconducting film placed at a distance h from the coil results to be $K_S(h) = \frac{1}{\mu_0} B_r^{TOTAL}(h) = \frac{1}{\mu_0} 2 \cdot \max\{B_r(h)\}$ where $B_r(h) = \mu_0 I_0 f(r, h) \cos(\omega t)$ is the radial component of the induction field generated by the coil at distance h in the absence of the sample. Applying the Bean's model, $K_S = J_C d$. By equaling the two expressions found for K_S , the scaling relation between the critical current density and the inducing coil current follows:

$$J_c = k \cdot \frac{I_{C0}}{d} \quad (1)$$

where I_{C0} is the inducing critical current (defined, for example, using a threshold criterion) and $k = 2 * \max\{f(r, h)\}$ is the coil factor.

In this paper we review this contactless technique by using a discrete modelisation for the current distribution in the coil, in order to calculate in an exact way the induction field in all the space as a function of the sample distance to the coil, thickness and magnetic penetration depth. We verify how and under which circumstance the assumptions made are verified in the framework of the model, and then we calculate the scaling coefficients linking the current circulating in the coil to the critical current density of the sample. The paper is organized as follows: in section II, after a brief overview on previous studies, we present the model and calculate the vector potential in all the space for the sample coil configuration; in section III we check the validity of our model comparing our analysis with similar results presented in literature; in section IV we present the experimental set-up used to measure superconducting samples of known transport properties to validate the analytical results; in section V we finally draw some conclusions.

II. THE DISCRETE MODEL

The Non Destructive Evaluation (NDE) of the conducting properties of metallic specimens by using eddy currents methods has been since years an important subject for the scientific community for both applicative and fundamental issues. As an example, we can cite the pioneering work by C. P. Bean⁵ that used a simple solenoid to measure the resistivity of a sample placed inside. The necessity of studying large area samples raised the problem of calculating the spatial profile of the induction field when using a small multiturn coil. This problem was solved in an original way by Dodd and Deeds⁶ with an "hybrid" model: they calculated the field profiles for a single turn coil and extended the result to the case of multiturn coils by integrating over the coil section. Their work has been the starting point for hundreds of experimental and theoretical studies in the field of NDE.

In the case of superconducting materials, the thin film technology raised the interest in the study of both the transport properties⁷ (the critical current density) and the electrodynamic

response (the absolute magnetic penetration depth)^{8,9,10,11,12,13,14,15} without damaging the sample under test. For these issues, a two coil configuration with both continuous and discrete approach has been used.

For a single coil configuration, a completely discrete approach by Gauzzi *et al*¹⁶ was used to model the coil impedance variation for the measure of the magnetic penetration depth of superconducting samples of different nature and shapes. Recently M. W. Coffey¹⁷ has reviewed the single and multiturn impedance coil problem by using a continuous method of kernel functions. For the evaluation of the transport properties of superconducting samples, we have shortly presented in the introduction the continuous model approach^{1,2}.

In this section, we extend the discrete model by Gauzzi *et al*¹⁶ to the calculation of the field induction profiles in all the space. We will show how and in which cases this exact model is simpler and more precise respect to previous hybrid or continuous models cited above.

We investigate the ac response of a superconducting slab of finite thickness situated at $-d < z < 0$, at a distance h from a pancake coil, as shown in figure 1. Further, we consider the hypothesis that the outer radius of the coil is less than half sample size to neglect edge effects. This will be better clarified in the following, when we will evaluate and show the magnetic field profiles.

First, we model the coil as a discrete distribution of concentric turns axially and radially¹⁶ equispaced. The wire is supposed infinitely thin; this assumption is valid when the wire diameter is much smaller than the skin depth at the working frequency. For example, in the case of a copper wire and at frequencies below MHz this approximation holds for wire diameter up to 0.1 mm. Thus the total current density circulating in the coil can be written in cylindrical coordinates in the following way:

$$J_{\theta,coil}(r, z) = I \sum_{n=0}^{N-1} \delta(z + h + n\Delta h) \sum_{m=0}^{M-1} \delta(r - R - m\Delta R) \quad (2)$$

where I is the total current flowing in the coil, δ is the delta function, R is the internal coil radius and Δh , ΔR are the spacings between N adjacent sheets and M adjacent turns in the same sheet respectively (see fig.1). We assume that Δh and ΔR both equals the wire diameter d_w .

Secondly, we consider the Maxwell equation at a frequency $\omega/2\pi$ for the vector potential

\vec{A} in the London gauge ($\vec{\nabla} \cdot \vec{A} = 0$), explicitly separating the contributions to the current density in the coil and in the sample:

$$\nabla^2 A_\omega = -\mu_0(j_{\omega,coil} + j_{\omega,sample}). \quad (3)$$

At low frequencies within the limit of validity of Ohm's law, the induced screening current in the sample can be expressed in the following way:

$$j_{\omega,sample} = i\omega\sigma_\omega A_\omega \quad (4)$$

where σ_ω is the frequency dependent complex conductivity of the sample. By inserting eq. 4 into eq. 3, the solution for the field A_ω becomes a function of $j_{\omega,coil}$ and σ_ω , the latter being the only free parameter.

To solve eq. 3, we note that the current density j_{coil} in the coil lies in the (x-y) plane of the sample. The same must be true for the induced screening currents in the sample, as in a mirror image. This consideration, and the assumption of a sample with isotropic conductivity σ in the plane, allow us to express eq. 3 in cylindrical coordinates. In this case, only the orthoradial component A_ϑ of the vector potential \vec{A} is non zero:

$$\nabla^2 A_\vartheta = -\mu_0(j_{\omega,coil} + iH_d(z)\omega\sigma_\omega A_\vartheta) \quad (5)$$

where the origin and direction of the z-axis are chosen as shown in figure 1, the ω -subscripts have been omitted, and $H_d(z)$ is the Heaviside function, whose value is unitary in the $[0,d]$ interval and zero elsewhere. We have solved the differential equation 5 in all the space with and without the sample by following the Pearl's formalism^{16,18}. The solution for the vector potential without the sample is:

$$A_\vartheta(r, z) = -\mu_0 \frac{I_0}{2} \int_0^\infty \left[\sum_n e^{-|z+h_n|\gamma} \sum_m r_m J_1(r_m \gamma) \right] J_1(r\gamma) d\gamma \quad (6)$$

In the presence of a superconducting sample we have three different solutions, corresponding to three different regions:

$z < 0$

$$A_{\theta}(r, z) = \mu_0 \frac{I_0}{2} \int_0^{\infty} \left[\sum_n e^{-|z+h_n|\gamma} \sum_m r_m J_1(r_m \gamma) \right] \cdot (1 - F(\gamma, z, d, l)) J_1(r\gamma) d\gamma \quad (7)$$

$$F(\gamma, z, d, l) = \frac{1}{1 + 2\gamma^2 l^2 + 2\gamma l \sqrt{1 + l^2 \gamma^2} \coth\left(\frac{d}{l} \sqrt{1 + l^2 \gamma^2}\right)} \quad (8)$$

$0 \leq z \leq d$

$$A_{\theta}(r, z) = -\mu_0 \frac{I_0}{2} \int_0^{\infty} \left[\sum_n \exp(-h_n \gamma) \sum_m r_m J_1(r_m m \gamma) \right] G(\gamma, z, d, l) J_1(r\gamma) d\gamma \quad (9)$$

$$G(\gamma, z, d, l) = \frac{2\gamma l \left[\gamma l \sinh\left(\frac{z-d}{l} \sqrt{1 + l^2 \gamma^2}\right) - \sqrt{1 + l^2 \gamma^2} \cosh\left(\frac{z-d}{l} \sqrt{1 + l^2 \gamma^2}\right) \right]}{(1 + 2\gamma^2 l^2) \sinh\left(\frac{d}{l} \sqrt{1 + l^2 \gamma^2}\right) + 2\gamma l \sqrt{1 + l^2 \gamma^2} \cosh\left(\frac{d}{l} \sqrt{1 + l^2 \gamma^2}\right)} \quad (10)$$

$z > d$

$$A_{\theta}(r, z) = -\mu_0 \frac{I_0}{2} \int_0^{\infty} \left[\sum_n e^{-h_n \gamma} \sum_m r_m J_1(r_m \gamma) \right] \cdot [1 - e^{-z\gamma} - L(\gamma, l, d) e^{-d\gamma}] J_1(r\gamma) d\gamma \quad (11)$$

$$L(\gamma, l, d) = \frac{2\gamma l \sqrt{1 + l^2 \gamma^2}}{(1 + 2\gamma^2 l^2) \sinh\left(\frac{d}{l} \sqrt{1 + l^2 \gamma^2}\right) + 2\gamma l \sqrt{1 + l^2 \gamma^2} \cosh\left(\frac{d}{l} \sqrt{1 + l^2 \gamma^2}\right)} \quad (12)$$

where γ is a wave number in the xy-plane, the functions F , G and L represent the sample contribution in the considered region, and J_0 and J_1 are the Bessel functions of order zero and one respectively. l is a complex length expressed by the formula:

$$l = \sqrt{\frac{i}{\mu_0 \omega \sigma_{\omega}}} \quad (13)$$

Note that it reduces to the normal skin depth for the case of normal metals and to the magnetic penetration depth for the case of superconductors. The radial and axial components of the magnetic field with and without the sample have been calculated from the vector potential by using the standard recursive relations:

$$B_r(r, z) = -\frac{\partial A_\vartheta}{\partial z} \quad (14)$$

$$B_z(r, z) = \frac{1}{r} \frac{\partial}{\partial r}(r A_\vartheta) \quad (15)$$

The explicit expressions for the components of the induction field in all the space are reported in appendix A.

III. NUMERICAL RESULTS

Our general model has been checked in the particular case of a single turn, single sheet coil by using the calculations of Dodd and Deeds⁶. In figure 2 we compare the results of the calculations of the radial (B_r) and axial (B_z) components of the induction field in the case of no sample for a single turn coil with inner radius $r_0=1$ mm and wire diameter equal to $50 \mu m$. The fields have been calculated at a distance $z = r_0$ from the coil surface ($z = 0$). The two models give the same result. In case of multi-turns coils, the continuous approach^{2,6} has been widely used. We point out that assuming the simple rectangular coil section of a continuous model produces an over-estimation of the effective area covered by the exciting coil current in respect to the discrete case, in which the effective surface is the sum of N-turn discs of the diameter of the coil wire. One would expect therefore an under-estimation of the maximum value of the magnetic field compared to the discrete case; the error decreases as the number of turns increases approaching the continuous limit. To show this, we compare the continuous^{2,6} and the discrete model calculating the radial component of the magnetic field in two cases: *a*) a coil of 5 turns, 5 sheets; *b*) a coil of 22 turns, 24 sheets. The inner radius r_0 is 1 mm and the sample to coil distance is $h=0.1$ mm; the wire diameter has been assumed to be $50 \mu m$. The results of these calculations are reported in figure 3. As expected, the maximum B_r field calculated with the continuous model is under-estimated respect to the discrete one of 8 and 2% for the case *a*) and *b*) respectively. By using the methods proposed in ref.^{1,2}, this would imply an under-estimation of the critical current density of the same amount.

Once the discrete model has been successfully tested, we have used it to calculate the coefficient $k(h)$ in eq. 1. Firstly, we have verified the condition to apply the Bean model

properly. To do so, we have calculated the total induction field on the sample surface by using eq. 9 and 14. The parameters used in this calculation are: the sample thickness $d=700$ nm, its magnetic penetration depth $\lambda = 250$ nm for a standard high quality YBCO sample^{13,19} at 77 K. For the probe coil we have considered a 22 turns, 24 sheets coil with the inner radius $r_0= 1$ mm and a wire diameter equal to $50 \mu\text{m}$. The results of this calculation are reported in figure 4: the normal component B_z is negligible in respect to the radial component B_r . Moreover, it is worthwhile to emphasize that the magnitude of B_r is about two times larger than in the case without sample shown in figure 3, in the same point of the space, as we can expect within the framework of a mirror image coil solution analysis. For the Bean model to be valid, the total induction field must be zero on the opposite side of the film. This is true when the effective screening length $\lambda_{\text{screening}}$ is equal to or less than the film thickness d . From eq. 8, in the case of a superconducting sample, it results $\lambda_{\text{screening}} = \lambda \cdot \coth(d/\lambda)$ ^{16,20}. When $\lambda_{\text{screening}} > d$ the error in the estimation of J_C may be very large: to estimate it roughly, we can calculate the relative difference in the J_C values when the film thickness equals d and the effective screening length $\lambda_{\text{screening}}$, i.e. $|1 - J_C(\lambda_{\text{screening}})/J_C(d)|$. For example, for a film with $d=200\text{nm}$ and $\lambda=250\text{nm}$, the error can rise up to 46%.

To calculate the coefficient k we take the maximum of the coil function $f(r)$ plotted in figure 3. This represents the spatial region where the field reaches its maximum value. In the case of the copper coil reported above, our discrete model gives the value of $k = 2 * 10^5 \text{m}^{-1}$ at a sample-coil distance $h=0.1$ mm. Our calculation allows to estimate $k(h)$ with an error of 2% for a minimum 10% error in the determination of h . $k(h)$ decreases as h increases as it is shown in figure 5, because of the presence of terms $\propto e^{-h\gamma}$ in the field expression. In the same graph, the experimentally determined values of k at various distance are also reported. The experimental values are in good agreement within the error bars with the behavior predicted by the discrete model. Details of the measurement will be given in the next section. The exact knowledge of the relation linking k to h makes this technique extremely flexible. For example, in the case of superconducting tapes or large area films, the probing coil must be moved all along the sample. Thus, to correctly estimate J_C , it is necessary to know exactly the magnetic coupling versus the sample to coil distance h .

IV. EXPERIMENTAL

To validate our discrete model we have inductively measured the critical current density of a superconducting film of well known transport properties. For the measure of the third harmonic signal V_3 we used a Lock-in amplifier (Signal Recovery 7265). The amplitude of the inducing sinusoidal current (the Lock-in reference signal) circulating in the coil is measured by using a high precision resistor in series with the coil. A commercial highly linear amplifier increases the inducing sinusoidal signal. The output signal is filtered by using a home made, low noise notch filter to reduce the first harmonic component noise and to avoid any saturation of the Lock-in. The temperature is monitored by a temperature controller (Neocera2021) connected to a Cernox resistor thermometer. The characteristics of the coil used in our experiment have been reported in the previous paragraph.

The samples tested are 700 nm thick YBCO thin films produced by Theva GmbH with dimensions $10 \times 10 \text{ mm}^2$. The critical temperature and the critical current density at liquid nitrogen temperature given by the producer are 87.9 K and 2.57 MA/cm^2 (expressed in root mean square) respectively. The value of the critical current I_{C0} was experimentally determined looking at the onset of non linearity by the extrapolation of the linear portion in the V_3 versus I plot (see for example in figure 6 and ref.¹). The value found for the critical current density of the sample of fig. 6 is $J_C = (2.6 \pm 0.3) \text{ MA/cm}^2$ at 77 K, in very good agreement with the data reported by the producer. For all the other samples tested, J_C has been found statistically well within the error bars of the measurement presented above. The error on I_{C0} is estimated as the difference between the first point that is no more aligned on the linear portion V_3 versus I and the extrapolated I_{C0} value (see the arrows on figure 6). This error is larger at low temperature because of the increase of the critical current density: at higher J_C , the noise level introduced by the amplifier is enhanced thus producing a rounding in the lossy state transition.

We have repeated the same experiment at different sample-coil spacings h , by using a micrometric screw with $10 \mu\text{m}$ resolution placed under the sample holder, to calculate the experimental scaling factor k vs h and comparing it to the expected theoretical behaviour. We note some important points: *i*) the experimental values have been obtained by considering the critical current density equal to the value given by the producer; *ii*) to minimize the error in the determination of the sample-coil distance, we have set the zero of the micromet-

ric screw when the sample is in contact with the coil ($h = 0\mu m$); *iii*) the error bars for $k(h)$ have been obtained by taking into account all the possible error sources (d and I_{C0}) whereas for h we have taken the minimum resolution of the micrometric screw. As one can see in figure 5, there is a very good agreement between the $k(h)$ values predicted by the discrete model and the experimental ones.

As a final test, we have plotted J_C versus T close to T_c in figure 7. The behaviour of the critical current density is a linear function of the temperature. This is usually explained as due to the presence of Josephson coupling between grains^{21,22}. A more detailed analysis of the $J_C(T)$ behaviour for $T > T_C/2$ goes beyond the scope of this work and will be presented elsewhere.

V. CONCLUSIONS

In this paper we have revisited in detail an inductive and contactless technique used for the measurement of the critical current density in superconducting films. The inductive geometric coupling factor has been calculated exactly by developing a precise and realistic model describing the current circulating in a real coil, and its image in a superconducting film placed in close contact to it. In particular, the scaling law of the geometric factor versus the sample-coil distance is found. This is a fundamental issue to render this technique flexible, in order to make possible a local non destructive evaluation of the critical current density in large areas films or superconducting tapes just moving a single probe coil at a known distance from the testing sample. This discrete analysis has been successfully verified by a comparison with similar continuous models presented in literature. The model presented here is more realistic, relatively simple and can describe the experimental data with a higher degree of precision in particular in the case of coils with a low number of turns contrarily to what happens using a continuous approach. The model has been verified experimentally by measuring the critical current density on YBCO films having well known transport properties.

Acknowledgments

We thank Dr. M. Valentino for fruitful discussions. We are grateful to Dr. V. De Luise, A. Maggio and S. Marrazzo for their valuable technical assistance.

*Corresponding author. E-mail address: gianrico.lamura@na.infn.it.

APPENDIX A: THE INDUCTION FIELD EXPRESSIONS

By using expressions (6-12), (14-15) and the recursive relation for the derivative of the Bessel functions we have calculated the radial and the normal induction field in all the space with and without the sample. The expressions are the following:

without the sample:

$$B_r(r, z) = \mu_0 \frac{I_0}{2} \int_0^\infty \left[\sum_n e^{-|z+h_n|\gamma} \sum_m r_m J_1(r_m \gamma) \right] J_1(r\gamma) \gamma d\gamma \quad (\text{A1})$$

$$B_z(r, z) = \mu_0 \frac{I_0}{2} \int_0^\infty \left[\sum_n e^{-|z+h_n|\gamma} \sum_m r_m J_1(r_m \gamma) \right] J_0(r\gamma) \gamma d\gamma; \quad (\text{A2})$$

One can define a geometric coil function² $f(r)$ for the radial component:

$$f(r) = \int_0^\infty \left[\sum_n e^{-h_n \gamma} \sum_m r_m J_1(r_m \gamma) \right] J_1(r\gamma) \gamma d\gamma. \quad (\text{A3})$$

with the sample:

$z < 0$

$$B_r(r, z) = -\mu_0 \frac{I_0}{2} \int_0^\infty \left[\sum_n e^{-|z+h_n|\gamma} \sum_m r_m J_1(r_m \gamma) \right] (1 - F(\gamma, d, l)) J_1(r\gamma) \gamma d\gamma \quad (\text{A4})$$

$$B_z(r, z) = \mu_0 \frac{I_0}{2} \int_0^\infty \left[\sum_n e^{-|z+h_n|\gamma} \sum_m r_m J_1(r_m \gamma) \right] (1 - F(\gamma, d, l)) J_0(r\gamma) \gamma d\gamma \quad (\text{A5})$$

$$0 \leq z \leq d$$

$$B_r(r, z) = \mu_0 \frac{I_0}{2} \int_0^\infty \left[\sum_n e^{-hn\gamma} \sum_m r_m J_1(r_m \gamma) \right] \frac{\partial G(\gamma, z, d, l)}{\partial z} J_1(r\gamma) d\gamma \quad (\text{A6})$$

$$B_z(r, z) = -\mu_0 \frac{I_0}{2} \int_0^\infty \left[\sum_n e^{-hn\gamma} \sum_m r_m J_1(r_m \gamma) \right] G(\gamma, z, d, l) J_0(r\gamma) \gamma d\gamma \quad (\text{A7})$$

$$\frac{\partial G(\gamma, z, d, l)}{\partial z} = \frac{2\gamma \left[\gamma l \sqrt{1 + l^2 \gamma^2} \cosh \left(\frac{z-d}{l} \sqrt{1 + l^2 \gamma^2} \right) - (1 + l^2 \gamma^2) \sinh \left(\frac{z-d}{l} \sqrt{1 + l^2 \gamma^2} \right) \right]}{(1 + 2\gamma^2 l^2) \sinh \left(\frac{d}{l} \sqrt{1 + l^2 \gamma^2} \right) + 2\gamma l \sqrt{1 + l^2 \gamma^2} \cosh \left(\frac{d}{l} \sqrt{1 + l^2 \gamma^2} \right)} \quad (\text{A8})$$

$$z > d$$

$$B_r(r, z) = \mu_0 \frac{I_0}{2} \int_0^\infty \left[\sum_n e^{-hn\gamma} \sum_m r_m J_1(r_m \gamma) \right] e^{-z\gamma} J_1(r\gamma) \gamma d\gamma \quad (\text{A9})$$

$$B_z(r, z) = -\mu_0 \frac{I_0}{2} \int_0^\infty \left[\sum_n e^{-hn\gamma} \sum_m r_m J_1(r_m \gamma) \right] \cdot [1 - e^{-z\gamma} - L(\gamma, l, d) e^{-d\gamma}] J_0(r\gamma) \gamma d\gamma \quad (\text{A10})$$

where $F(\gamma, z, d, l)$, $G(\gamma, z, d, l)$ and $L(\gamma, d, l)$ have been defined in eq. 8, eq. 10 and eq. 12 respectively.

Finally, it is possible to evaluate exactly the maximum electric field induced on the surface of the sample ($z=0$). By using the third Maxwell equation and eq. 9 we have:

$$E_\vartheta(r, z) = \max \left\{ -\frac{\partial A_\vartheta}{\partial t} \right\} = \mu_0 I_0 \omega \max \{f(r)\} \quad (\text{A11})$$

¹ J. H. Claassen, M. E. Reeves, and R. J. Soulen, Rev. Sci. Instrum. **62**, 996 (1991).

² Y. Mawatary, H. Yamasaki, and Y. Nakagawa, Appl. Phys. Lett. **81**, 2424 (2002).

³ Y. Mawatary, H. Yamasaki, and Y. Nakagawa, Appl. Phys. Lett. **83**, 3972 (2003).

⁴ H. Yamasaki, Y. Mawatary, and Y. Nakagawa, Appl. Phys. Lett. **82**, 3275 (2003).

- ⁵ C.P.Bean, J. Appl. Phys. **30**, 1976 (1959).
- ⁶ C. V. Dodd and W. E. Deeds, J. Appl. Phys. **39**, 2829 (1968).
- ⁷ H. Hochmuth and M. Lorentz, Physica C **71**, 339 (1992).
- ⁸ A. T. Fiory, A. F. Hebard, P. Mankiewich, and R. E. Howard, Appl. Phys. Lett. **52**, 2165 (1988).
- ⁹ B. Jeanneret, J. L. Gavilano, G. A. Racine, C. H. Leemann, and P. Martinoli, Appl. Phys. Lett. **55**, 2336 (1989).
- ¹⁰ Z.-H. Lin, G. C. Spalding, A. M. Goldman, B. F. Bayman, and O. T. Valls, Eurohys. Lett. **32**, 573 (1995).
- ¹¹ S. J. Turneaure, E. R. Ulm, and T. R. Lemberger, J. Appl. Phys. **79**, 4221 (1996).
- ¹² J. Y. Lee, Y. H. Kim, T. S. Han, and S. S. Choi, Appl. Phys. Lett. **69**, 1637 (1996).
- ¹³ A. Fuchs, W. Prusseit, P. Berberich, and H. Kinder, Phys. Rev. B **53**, R14745 (1996).
- ¹⁴ J. H. Claassen, M. L. Wilson, J. M. Byers, and S. Adrian, J. Appl. Phys. **82**, 3028 (1997).
- ¹⁵ M. W. Coffey, J. Appl. Phys. **87**, 4344 (2000).
- ¹⁶ A. Gauzzi, J. L. Cochee, G. Lamura, B. J. Jönsson, V. A. Gasparov, F. R. Ladan, B. Placais, P. A. Probst, D. Pavuna, and J. Bok, Rev. Sci. Instr. **71**, 2147 (2000).
- ¹⁷ M. W. Coffey, J. Appl. Phys. **220**, 209 (1994).
- ¹⁸ J. Pearl, Ph.D. thesis, Polytechnic Institute of Brooklyn, New York (1965).
- ¹⁹ K. M. Paget, B. R. Boyce, and T. R. Lemberger, Phys. Rev. B **59**, 6545 (1999).
- ²⁰ W. H. Chang, J. Appl. Phys. **50**, 8129 (1979).
- ²¹ J. Halbritter, J. Appl. Phys. **71**, 339 (1992).
- ²² J. C. Nie, H. Yamasaki, Y. Nakagawa, K. Develos-Bagarinao, M. Murugesanand, H. Obara, and Y. Mawatari, Appl. Phys. Lett. **86**, 192507 (2005).

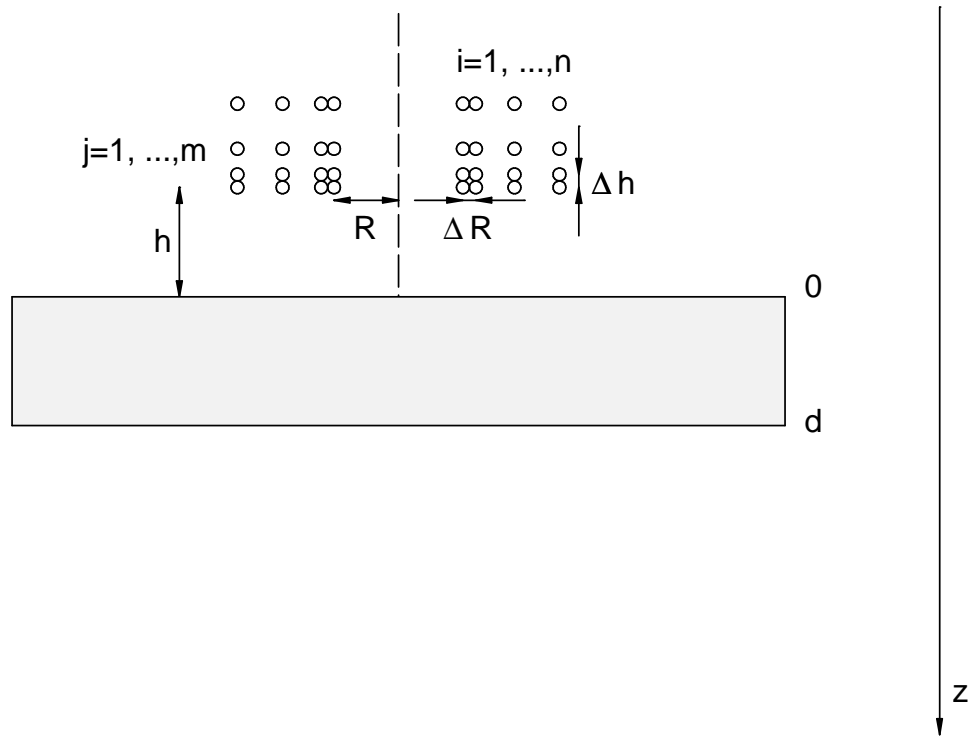


FIG. 1: Section of the sample-coil configuration. The coil is modelled as a discrete distribution of concentric turns axially and radially equispaced. h is the sample-coil distance and d is the sample thickness. Δh and ΔR are the spacings between N adjacent sheets and M adjacent turns in the same sheet respectively.

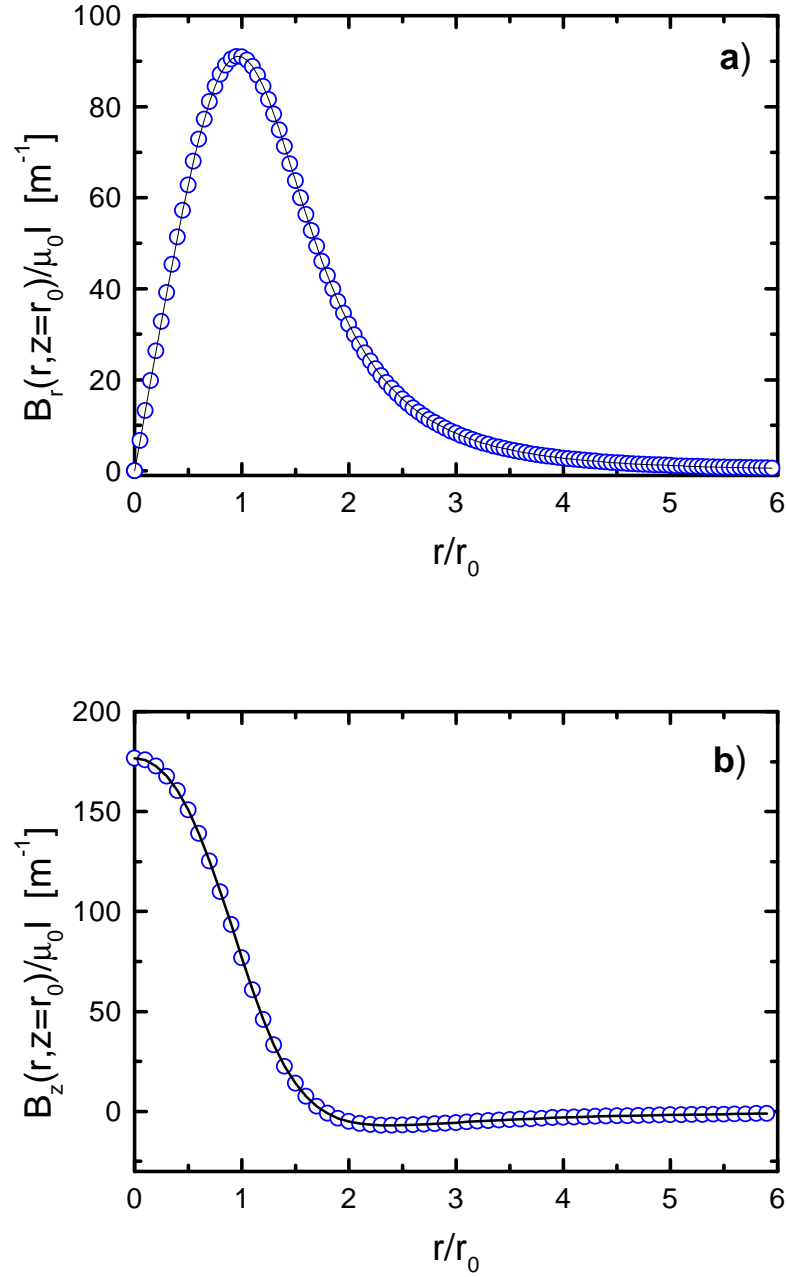


FIG. 2: (Color Online) a) radial component $B_r(r, z = r_0)$ of the induction field for a one turn one sheet coil calculated by using the Dodd and Deeds's model (continuous line) and our discrete model (open circles) respectively as a function of r/r_0 ; b) the same as in a) for the normal component $B_z(r, z = r_0)$.

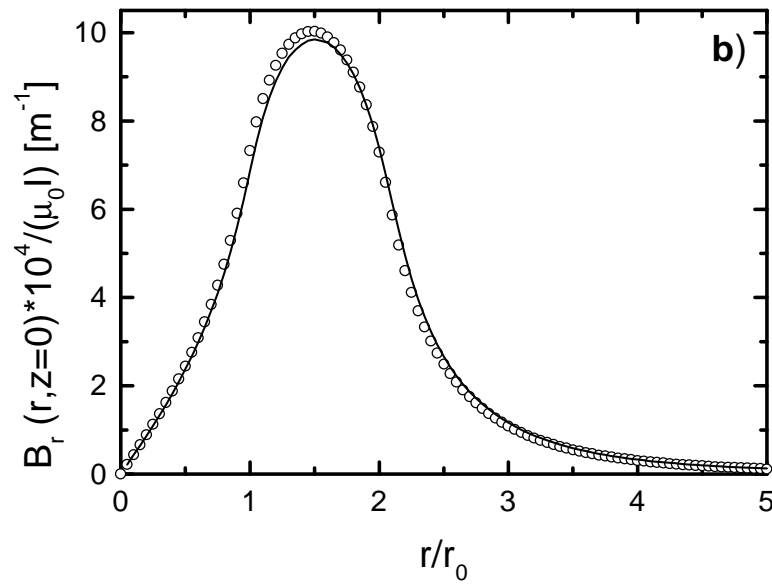
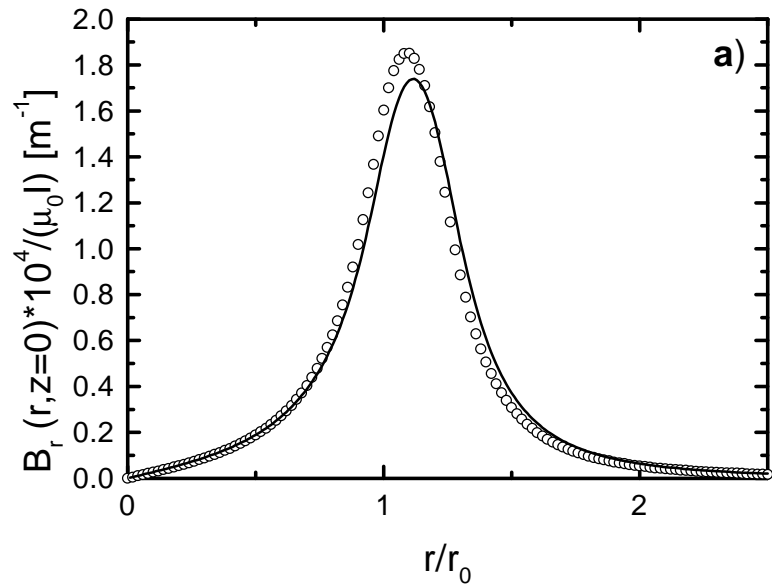


FIG. 3: Radial component of the magnetic field for the two coils of cases *a*) and *b*). The open circles and the lines represent the discrete and the continuous model respectively.

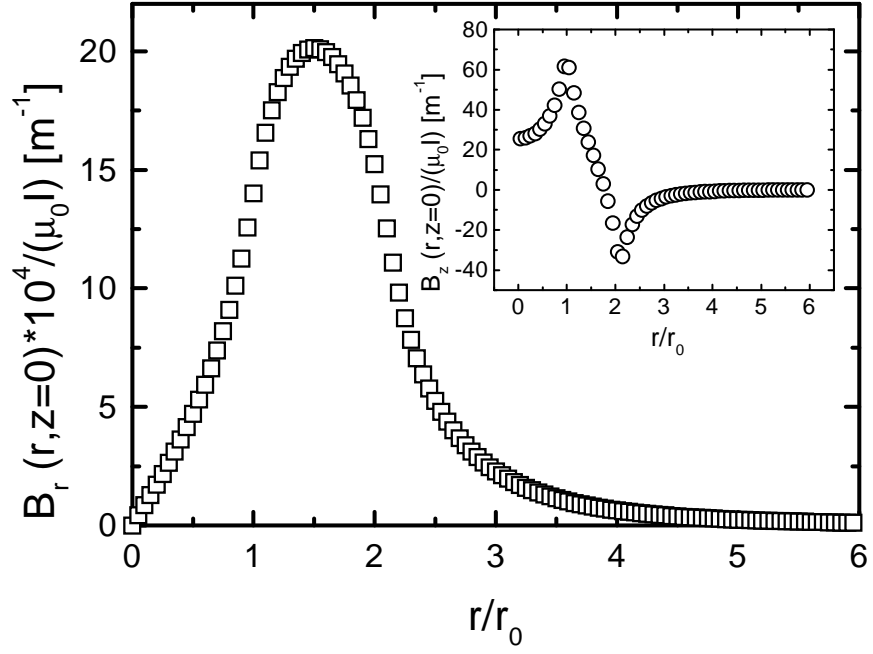


FIG. 4: Radial component of the total induction field (open squares) for a multi-turn coil. In the inset the result for the normal component (open circles) is shown. Both components have been calculated at the sample surface as a function of r/r_0 .

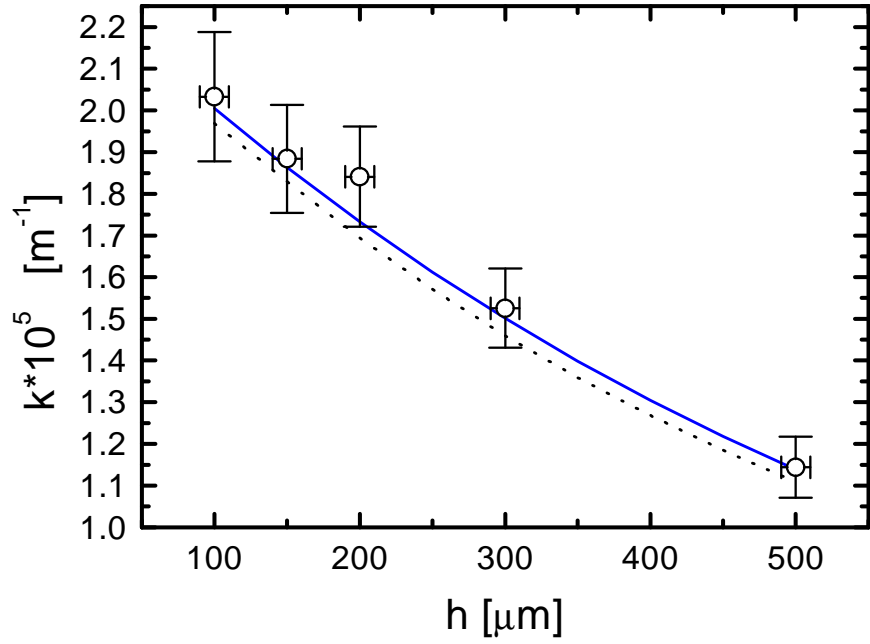


FIG. 5: (Color Online) Determination of the scaling factor k versus the sample to coil distance h . The continuous and the dashed lines represent the behaviour expected for the discrete and the continuous model respectively. The open circles represent the k -values experimentally evaluated.

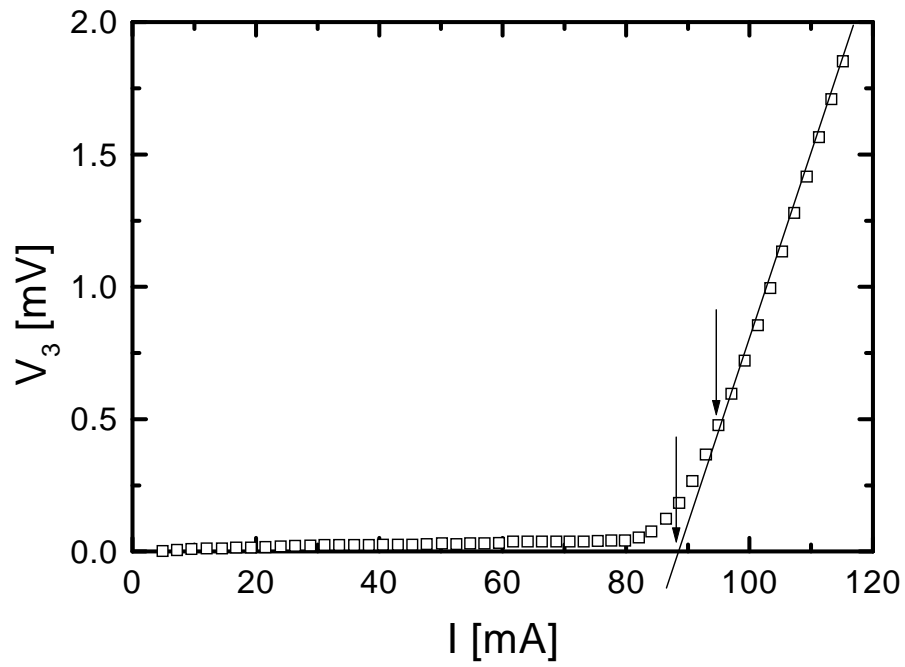


FIG. 6: Determination of the critical current I_{C0} . The arrow indicates the last point below which the third harmonic voltage is no more linear as a function of I .

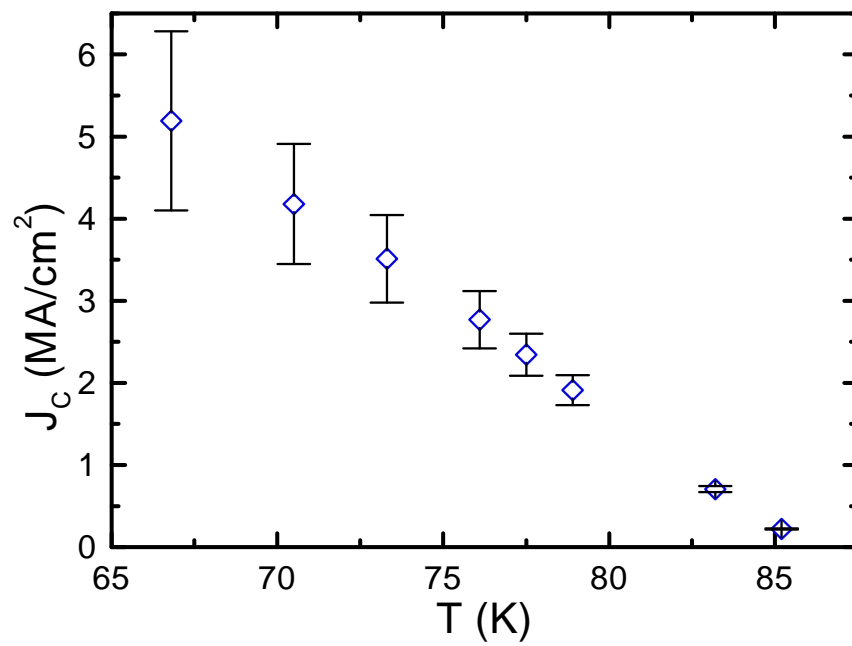


FIG. 7: (Color Online) Critical current density J_C versus temperature for a YBCO thin film.